Intermittent dynamics underlying the intrinsic fluctuations of the collective synchronization patterns in electrocortical activity

Pulin Gong, Andrey R. Nikolaev, and Cees van Leeuwen
Laboratory for Perceptual Dynamics, Brain Science Institute, RIKEN, Wako-Shi, Saitama, 351-0198, Japan
(Received 17 June 2005; revised manuscript received 9 January 2007; published 11 July 2007)

We investigate patterns of collective phase synchronization in brain activity in awake, resting humans with eyes closed. The alpha range of human electroencephalographic activity is characterized by ever-changing patterns, with strong fluctuations in both time and overall level of phase synchronization. The correlations of these patterns are reflected in power-law scaling of these properties. We present evidence that the dynamics underlying this fluctuation is type-I intermittency. We present a model study illustrating that the scaling property and the collective intermittent dynamics are emergent features of globally coupled phase oscillators near the critical point of entering global frequency locking.

DOI: 10.1103/PhysRevE.76.011904 PACS number(s): 87.19.La, 05.45.Xt, 05.70.Fh

I. INTRODUCTION

Synchronization is a fundamental phenomenon in coupled nonlinear oscillators and is encountered in physical and chemical as well as biological systems [1]. In particular, it is a commonly observed phenomenon in the neurosciences [2]. Synchronization processes in brain activity have been studied at all levels, ranging from single neurons to the whole cortex. Notably, at all these levels synchronization is governed by a high degree of spatiotemporal fluctuation; various patterns of synchronized and desynchronized activity emerge and disappear over time; brain activity appears to be switching between these states perpetually. Such behavior has been observed in neural responses to external stimulation as well as in ongoing spontaneous activity [3–8]. Especially, the latter shows highly variable coherence structures that are believed to reflect the endogenous states of the brain [9–11] and play important roles in shaping the former [12]. Fluctuations in neural synchrony are therefore of considerable scientific interest.

Here, we raise the following basic question: can we identify a dynamic mechanism that can be held responsible for the intrinsic fluctuations in spontaneous patterns of neural activity? We address this question by investigating collective phase synchronization in spontaneous activity as found in the alpha range of the human electroencephalogram (EEG) (8–13 Hz). Alpha-range activity is the most ubiquitous and robust rhythm observed in EEG. Several recent studies have described collective phase synchronization in this activity range [13,14]. However these studies concentrated on phase patterns occurring during global phase synchronization, whereas these states are, in fact, alternated with episodes of more irregular activity. Our present investigation, therefore, treats phase synchronization patterns, including synchronization and desynchronization periods, as a stream of ongoing activity.

Our investigation starts out by showing that whole-head, pairwise phase synchronization patterns show power-law scaling behavior, reflecting the strong long-range coherences of these patterns. Their ever-changing stream, therefore, has an underlying dynamics that, as we will show next, has the property of type-I intermittency. This kind of dynamics enables the brain to rapidly enter and exit different synchronized states, rendering synchronized states metastable.

In order to understand how the intermittent dynamics can emerge as a collective phenomenon in electrocortical rhythmic activity, we explain our data in terms of a physical model of globally coupled phase oscillators [15]. This model, even though it is simple and possesses only few design assumptions, has previously been used to explain the emergence of coherence in actual physical systems [16]. Comparing the collective properties of phase patterns in the model to those observed in alpha activity, we find that the model accounts for the scaling property and qualitatively reproduces the intermittent dynamics. In particular, we obtain this result when the model is poised, close to a critical point of entering a global frequency locking state. This result, therefore, suggests that criticality might be essential for the collective dynamics found in spontaneous brain activity.

II. PHASE SYNCHRONIZATION ANALYSIS

Our study is focused on spontaneous alpha-range activity (8–13 Hz) in human EEG [17]. Measurements were performed on eight healthy normal subjects of ages 18–30. Subjects were seated in a comfortable armchair in a light-attenuated and magnetically shielded room and were asked to relax with eyes closed. EEG was recorded from 64 channels using the Neuroscan system during a 6-min session. Linked ears were used as reference. To eliminate the effects of volume conduction, we uniformly choose 22 channels out of the 64 channels. These channels have maximally long distances between each other. In a preanalysis, we found that all subjects have strong alpha frequency.

To obtain phase synchronization data from the EEG signals, the complex Morlet wavelet is used. Specifically, for a signal recorded by the kth electrode, $S_k(t)$, the wavelet coefficients are described as

$$W_{S_k}(t_0,a)=\frac{1}{a}\int_{-\infty}^{+\infty}S_k(t)\psi^*\left(\frac{t-t_0}{a}\right)dt,$$

where $\psi^*\left(\frac{t-t_0}{a}\right)$ is the complex conjugate of the Morlet wavelet defined as Eq. (1) and a is the wavelet scale [18]:

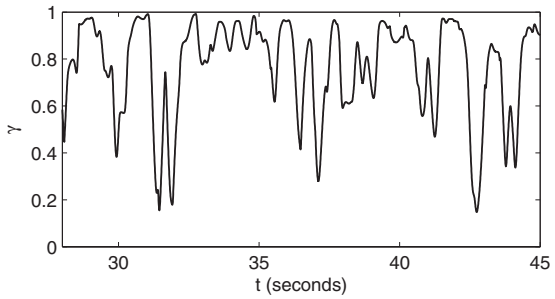

FIG. 1. Synchronization index over time for a single pair of channels chosen from prefrontal and occipital parts of the brain.

$$\psi(t) = \pi^{-1/4} e^{6it} e^{-t^2/2}. \quad (1)$$

The wavelet coefficient can be described by $W_{S_k}(t_0,a) = A_k(t_0,a)e^{i\phi_k(t_0,a)}$, where $A_k(t_0,a)$ and $\phi_k(t_0,a)$ represent amplitude and phase, respectively. The wavelet method can be applied to any frequency ranges we are interested in and is suitable for nonstationary time series [19]. Noise can cause phase slips, so phase synchronization for noisy systems has the following features: the relative phase difference $\psi_{k,l}(t,a) = |\phi_k(t,a) - \phi_l(t,a)|$, instead of being fixed, hovers around a constant value, and the distribution of the relative phase difference in the unit circle has a peak. Phase synchronization can be treated only in a statistical sense by detecting the appearance of significant peaks. This can be done by comparison with surrogate data [20]. We apply a sliding window of length n to obtain the phase synchronization index $\gamma_{k,l}(t,a)$ between the kth channel and lth channel. The first Fourier mode of the distribution of the relative phase difference is used as the phase synchronization index:

$$\gamma_{k,l}(t,a) = \left(\left\{ \frac{1}{n+1} \sum_{j=-n/2}^{n/2} \sin[\psi'_{k,l}(t+j\Delta t,a)] \right\}^2 + \left\{ \frac{1}{n+1} \sum_{j=-n/2}^{n/2} \cos[\psi'_{k,l}(t+j\Delta t,a)] \right\}^2 \right)^{1/2}, \quad (2)$$

where $\Delta t = 0.002$ s is the sampling time step, $n = 250$. By adjusting the value of the wavelet scale a, the wavelet is centered at the peak of the alpha frequency range, 8–13 Hz, determined individually from the average amplitude spectra for each subject. Phase synchronization indices range from 0 to 1 with 1 indicating perfect phase locking.

To reduce spurious detection of phase synchronization, we derive a significance level for each synchronization index by applying our analysis to two kinds of surrogate data. The first one is obtained by generating, for every subject, 100 pairs of independent white noise signals, each having the same length as the original data. The second one is generated according to the method described in Ref. [21], with the same number of pairs as used for the real EEG data. This method is designed for multichannel time series and can preserve both the power spectra and the cross spectrum of the original data. After wavelet transforms in the alpha-frequency range, phase synchronization indices are obtained for all surrogate data. These indices for both surrogate data

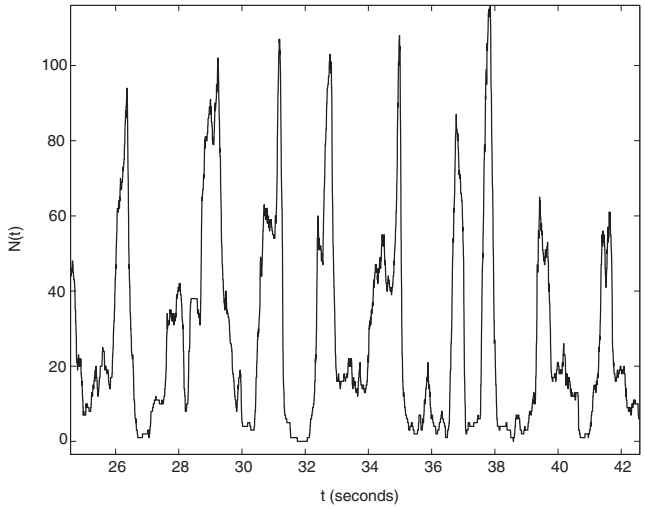

FIG. 2. Measure of global order in spontaneous alpha EEG: the total number of phase synchronized pairs of channels as a function of time.

are pooled together to form a distribution. We use the 99th percentile of the distribution as the significance level $\gamma'_{k,l}$; its values vary according to subjects. Relevant values of the synchronization indices are obtained by subtracting the 99th percentile values of the surrogate series: $\gamma^S_{k,l}(t,a) = \max\{\gamma_{k,l}(t,a) - \gamma'_{k,l}, 0\}$. The resulting value is the significant phase synchronization index. Values larger than zero indicate significant phase synchronization between the kth and lth channels at time moment t. Figure 1 shows the fluctuation and variability of the phase synchronization index over time for one arbitrary electrode pair. Since we are interested in the collective dynamics of the phase synchronization patterns, we count for each time step the total number of synchronized pairs. The 22 selected channels yield a total of 231 pairs. Of these, we consider the ones that show synchronized activity at a given point in time. The total number of these pairs constitutes our global order measure. It is denoted by $N(t)$. As shown in Fig. 2, there are moments in time where this measure indicates a high degree of synchronization, or order, as well as intervals where desynchronized, or disordered, activity predominates. Thus, the time series of $N(t)$ nicely reflects the global order of the brain states, providing us with a clear description of the intrinsic fluctuations in the patterns of phase synchrony.

III. COLLECTIVE PROPERTY AND DYNAMICS UNDERLYING FLUCTUATING PHASE SYNCHRONIZATION PATTERNS

We now turn to investigate the properties of the fluctuations in the synchronized phase patterns and reveal the underlying mechanism. First, the distribution of the global order measure $N(t)$, as shown in Fig. 3, has a linear part in the log-log plot. The exponent for the linear part, extracted with the maximum-likelihood method [22], is −1.65, and this linear part is followed by a fast cutoff part which is due to finite-size effects. As shown in Fig. 3, there is a clear dis-

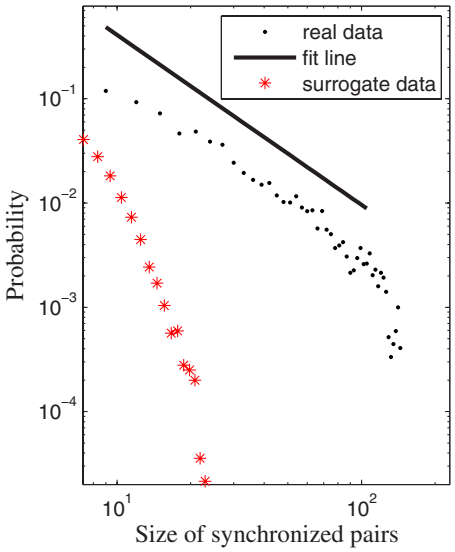

FIG. 3. (Color online) The distribution of the number of synchronized pairs for real data and surrogate data. The solid line represents the maximum-likelihood fit of the linear part of real data.

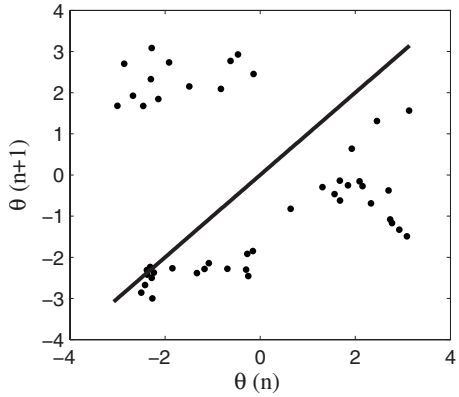

FIG. 4. One-dimensional map of angles $\theta(n+1)$ versus $\theta(n)$. The dashed line represents the bisectrix $\theta(n+1)=\theta(n)$. Data from one typical subject.

crepancy between real recordings and surrogate data, which hints at the presence of a nonrandom component in the collective synchronized activity patterns.

We next seek to clarify the dynamic mechanism underlying the nonrandomness of the fluctuations in the synchronized patterns. We use a method consisting of two main steps: (i) we construct from the time series of the global order measure $N(t)$ a return times map; (ii) we construct a map of angles based on the return times map. The return times for a given dynamical system with observed signal $x(t)$ are defined as the time intervals between successive crossings in the same direction of $x(t)=c$, with constant c. According to Takens' theorem and its extension, the system dynamics can be reconstructed from its one-dimensional time series [23] and in particular, as has been shown theoretically, from return times series [24]. Most recently, the methods based on the angles map of return times have been improved and used for the detection of deterministic structure in time series data of real biological systems [25,26]. Our method is solidly based on the method used in [25,26]. Note that, in order to construct a map of angles based on a one-dimensional time series, instead of a return times map, a Poincaré map is often used. For example, consider the method of extracting a map of angles from Couette-Taylor flow [27]. However, when it is difficult to obtain the secant hypersurface for a Poincaré section, the intervals map could be used instead [25].

For a given dynamical system with observed signal $x(t)$ the return times are defined as the intervals between successive crossings in the same direction of $x(t)=c$, for a given constant c. We calculate the time moments, denoted as $t(i)$, $i=1,n$, when $N(t)$ crosses a constant value N_c in the positive direction and obtain the return time series $T(i)=t(i+1)-t(i)$. We present results for $N_c=80.5$; our conclusions, however, remain valid for threshold values ranging from 91st to 96th percentile of the distribution of $N(t)$. To obtain the angles map we represent the mean value of $(T(i+1),T(i))$ in x, y coordinates as the central point in the return map. We determine the angle of the vector from this center for each point $(T(i+1),T(i))$ of the map. Angles are denoted by $\{\theta(i),\ i=1,M_1\}$. From this, the map of the angles $(\theta(i+1),\theta(i))$ is constructed. Figure 4 illustrates the result for one subject. Very similar results are obtained when the same analysis is performed on any of the other seven subjects. As shown in this figure, the map has a clear structure. In particular, it possesses segments that are fuzzily tangential to the bisectrix, or main diagonal. Maps that have fuzzy diagonal tangency are a feature of type-I intermittency in experimental data with noise [28].

We proceed in the investigation of intermittent dynamics by looking at the probability distribution of the laminar phases, the parts with small amplitude and relative small fluctuations as shown in Fig. 2. The laminar intervals are interrupted in an irregular way by bursting activity. We consider the distribution of the laminar intervals by imposing a threshold value which can range from 80th to 89th percentile of the distribution of $N(t)$. Figure 5 shows a log-log plot of the probability distribution $P(\tau)$ of the laminar intervals τ. There is a clear power law relationship in this distribution extending over two orders of magnitude. The corresponding exponent calculated by using the maximum-likelihood method is -1.61. As has been shown theoretically [29], a power-law distribution of the laminar phases is a property of intermittent maps. The result, therefore, provides us with additional evidence of intermittency in our data.

IV. SURROGATE DATA ANALYSIS

The intermittent dynamics describes the alternation of regular, low-variance and irregular, high-variance activity as a consequence of dynamical structure. We test the significance of the proposed intermittent dynamics against the null hypothesis that the fluctuations in variance are due to random volatility clustering behavior, meaning that the variance is high in one episode and low in the next. To this purpose we use the autoregressive conditional heteroskedasticity (ARCH) process [30] to generate surrogate data. As shown in Fig. 6, ARCH processes can generate random volatility clus-

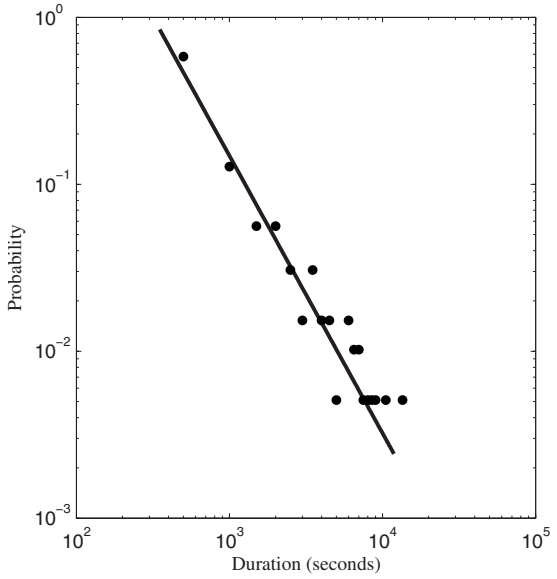

FIG. 5. Log-log plot of the probability distribution $P(\tau)$ of the laminar phase intervals τ obtained from the EEG data. Data from one typical subject.

tering. For each time, 231 pairs of ARCH independent random processes are generated. After obtaining for these pairs the synchronization index by using the wavelet method, a threshold is applied corresponding to the same percentile point as in the analysis for real data in the distribution of the synchronization index to obtain a surrogate time series of numbers of significantly synchronized pairs, $N(t)$, as in the above analysis. We continue the procedure for analyzing surrogate data in the same way as for real EEG data. We perform the analysis for 1000 groups of surrogate data (each group consists of 231 pairs). As shown in Fig. 3, the surrogate data yield a distribution for the sizes of pairwise synchronization that differs significantly from our data. We find that in total six out of eight subjects significantly ($p<0.05$) show the diagonal tangency exemplified in Fig. 4. These results, therefore, support the conclusion that the intermittent dynamics underlying the behavior of collective phase synchronization is an intrinsic feature of the EEG alpha-range activity.

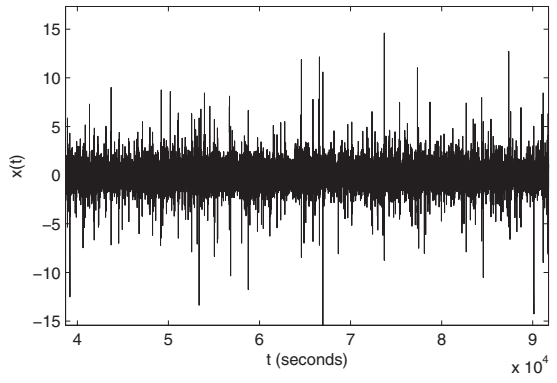

FIG. 6. Time series generated by the ARCH process, with the volatility clustering property.

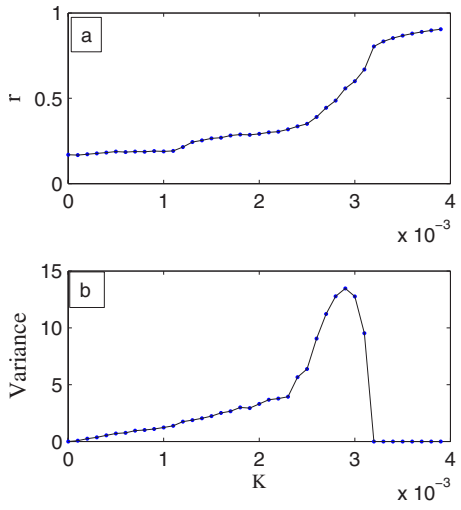

FIG. 7. (Color online) (a) Order parameters for the Kuramoto model as a function of coupling strength. (b) Variance of the number of synchronization pairs. The variance has a maximum at the critical point of entering global frequency locking for $K_c = 0.002\,89$.

V. MODEL AND COLLECTIVE PROPERTY OF SYNCHRONIZED PATTERNS OF GLOBALLY COUPLED PHASE OSCILLATORS

Synchronization in brain activity involves a large variety of physical and biochemical processes, many of which are only partially known. In such a case, it may be useful to consider the simplest possible physical model capable of qualitatively reproducing the collective features revealed in the data. To this aim, we propose a Kuramoto model of globally coupled phase oscillators. The model is described as follows [15,16]:

$$\dot{\theta}_i = w_i + \frac{K}{N}\sum_{j=1}^{N} \sin(\theta_j - \theta_i), \tag{3}$$

where w_i is the frequency of the ith oscillator, K is the coupling strength, and N is the total number of elements in the system. Consistently with our data, we used $N=22$. Frequencies w_i are drawn from a normal distribution with zero mean and variance 0.0015.

The order parameter $r(t)=|\frac{1}{N}\Sigma_{j=1}^{N} e^{i\theta_j(t)}|$ carries information about the level of phase synchronization produced by the model, and a variance measure is defined as $\mathrm{var}(N(t)) = \langle |N(t) - \langle N(t)\rangle|^2\rangle^{1/2}$ with $N(t)$ calculated using Eq. (2) in the manner as for the experimental data. This measure expresses variability in terms of the number of synchronized pairs and therefore is easy to compare with our experimental results. A measure similarly based on the variance of the number of synchronized clusters has been used to discriminate different collective patterns in coupled nonlinear oscillators and detect transition points for entering a fully synchronized state from partially synchronized ones [31]. The whole system was simulated with 0.0005 time intervals for a total of 90 000 000 steps; the first 6 000 000 steps were discarded as transient states.

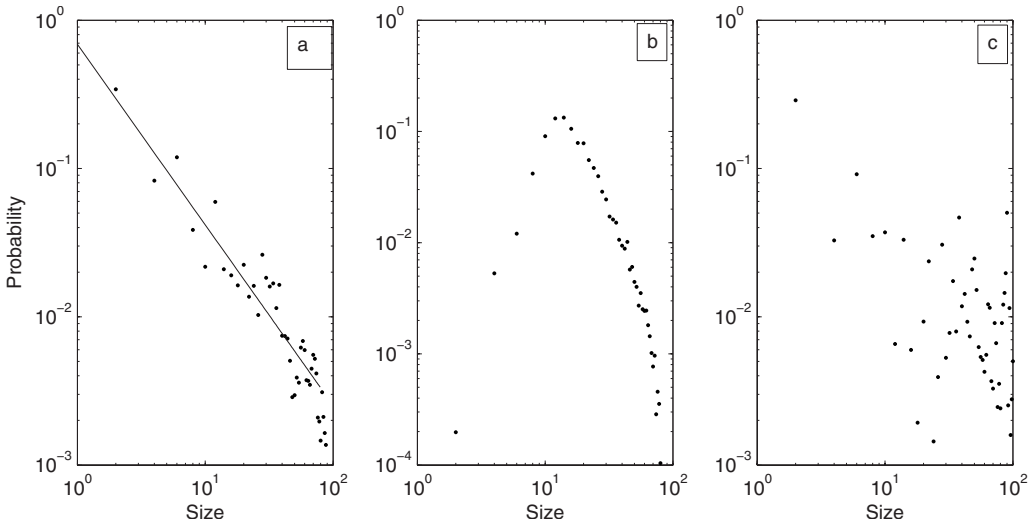

FIG. 8. The distribution of the number of pairwise synchronizations for the model with different values of coupling strength K: (a) $K=K_c=0.00289$, (b) $K=0.0020<K_c$, and (c) $K=0.00292>K_c$.

Figure 7 shows the mean value $\langle r\rangle$ and variance of pairwise synchronization var$(N(t))$ over the chosen time interval as a function of coupling strength K. We observe that the variance is maximal at the critical point of entering global frequency locking—in other words, on entering from partial phase-locking states to fully phase-locking states. As shown in Fig. 7(b), this critical point is found at $K_c=0.002\,89$.

We investigate for the model—first, the scaling property of $N(t)$, the number of pairwise phase synchronization, which is calculated in Eq. (2) with $n=700$, and a threshold near 1.0. Figure 8 shows a log-log plot of the distribution of this number. For the parameter near the critical point $K_c=0.002\,89$, this distribution is characterized by a linear part followed by a fast cutoff part, the same as for our experimental data. This result for the model is obtained only when the system is near the critical point, with $K=K_c$; as shown in Figs. 8(b) and 8(c), other values of K which are chosen away from the region near the critical point do not result in scale invariance for the distribution of the number of synchronized pairs.

Next, we describe for the model the collective dynamics of the patterns of phase synchronization, using the same method as for our experimental data. Starting from model time series $N(t)$, we obtain the angles map shown in Fig. 9. When $K=K_c=0.002\,89$—i.e., when the coupling strength is tuned near the critical point—the resulting map clearly has a diagonal tangency [Fig. 9(a)]. As a consequence, the return times have alternating laminar and bursting phases. In other words, the system shows intermittent dynamics as an emergent characteristic of the globally coupled phase oscillators near the critical point. When, by contrast, coupling parameters away from the critical point are chosen, there is no evidence of such dynamics. Values lower than K_c, shown for $K=0.002$ in Fig. 9(b), result in less-organized, noisy dynamics, and values greater than K_c, as shown for $K=0.002\,98$ in Fig. 9(c), result in a fuzzy fixed point. In order to reproduce

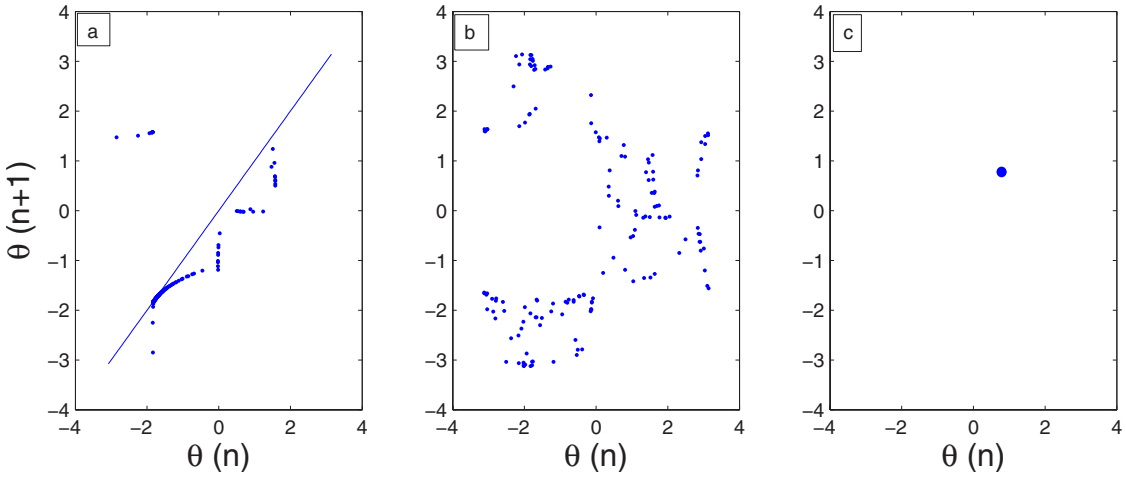

FIG. 9. (Color online) The map of angles $\theta(n+1)$ versus $\theta(n)$ for the Kuramoto model (a) with $K=K_c$—i.e., near the critical point of the phase transition. Note that the map has a part that is tangential to the bisectrix around the point $(-1.85,-1.85)$. (b) $K=0.002<K_c$, (c) $K=0.00298>K_c$.

in the model the scaling property of the number of synchronized pairs and the intermittent dynamics that produces it, the coupling parameter must therefore be tuned close to the critical point.

VI. CONCLUSION AND DISCUSSION

We have identified a collective intermittent dynamics underlying the spontaneous phase synchronization processes of EEG alpha-range activity. The intermittent dynamics enables the synchronized states to be metastable. Such dynamics engenders rapid switching between different synchronized states, without becoming trapped in any one stable state. Thus, the beneficial effect of the intermittent dynamics is that it provides the brain with a flexibility to respond to the greatest variety in stimulation. Such flexibility may be crucial for neural systems to represent and process information [32,33].

We have shown that a model of globally coupled phase oscillators poised very close to a critical point can qualitatively reproduce the intermittent dynamics and the power-law scaling of synchronization. As compared with the real, neurophysiological sources of EEG rhythms and their synchronization behavior, the present model is extremely simplified. The observation that a physical model based on minimal design assumptions is capable of simulating these biological data in great detail illustrates that abstract physical models may contribute significantly to our understanding of the basic working mechanisms of real neural systems. In a similar spirit, recently Ising models have been used to interpret neural spiking patterns [34].

For the present model, the only specific assumption we made is that coupling strength remains near a critical point. The model studies, therefore, suggest the relevance of criticality for generating highly variable phase synchronization patterns in neural systems. Note that for equilibrium statistical systems at the critical point of the phase transition, intermittency has been found recently [35,36]. Interestingly, the collective dynamics of a type of intermittent dynamics characterized by the diagonal tangency for cellular automata has also been found in the state of transition from order patterns to chaotic patterns [37]. All these provide an analogy to our results. We may conclude that spontaneous phase synchronization patterns in EEG alpha-range signals could be understood in terms of coupled nonlinear oscillators at the critical point. Fine-tuning of criticality as required in the model, however, appears unlikely for our brain. We therefore assume that this criticality is self-organized [38].

Criticality in brain rhythms has been investigated from a statistical perspective, by analyzing the power spectra of individual recording sites. Here we illustrate the criticality of brain activity from a different perspective, based on the collective property of synchronized patterns in brain activity and their dynamical origins. The findings are supportive for casting a dynamical systems perspective on the highly variable and ever-changing spontaneous patterns in neural activity.

[1] A. Pikovsky, M. Rosenblum, and J. Kurths, *Synchronization: A universal concept in nonlinear sciences* (Cambridge University Press, Cambridge, England, 2001).
[2] W. Singer, Neuron **24**, 49 (1999).
[3] C. M. Gray, A. K. Engel, P. Konig, and W. Singer, Visual Neurosci. **8**, 337 (1992).
[4] E. Rodriguez *et al.*, Nature (London) **397**, 430 (1999).
[5] A. Riehle, S. Grun, M. Diesman, and A. Aertsen, Science **278**, 1950 (1997).
[6] S. L. Bressler, R. Coppola, and R. Nakamura, Nature (London) **366**, 153 (1993).
[7] T. H. Bullock *et al.*, Proc. Natl. Acad. Sci. U.S.A. **92**, 11568 (1995).
[8] P. Gong, A. R. Nikolev, and C. van Leeuwen, Neurosci. Lett. **336**, 33 (2003).
[9] I. Lampl, I. Reichova, and D. Ferster, Neuron **22**, 361 (1999).
[10] M. Tsodyks, T. Kenet, A. Grinvald, and A. Arieli, Science **286**, 1943 (1999).
[11] T. Kenet *et al.*, Nature (London) **425**, 954 (2003).
[12] J. Fiser, C. Chiu, and M. Weliky, Nature (London) **431**, 573 (2004).
[13] P. L. Nunez, B. M. Wingeier, and R. B. Silberstein, Hum. Brain Mapp. **13**, 125 (2001).
[14] J. Ito, A. R. Nikolaev, and C. van Leeuwen, Biol. Cybern. **92**, 54 (2005).
[15] Y. Kuramoto, *Chemical Oscillations, Waves, and Turbulence* (Springer, Berlin, 1984).
[16] J. A. Acrbron *et al.*, Rev. Mod. Phys. **77**, 137 (2005).
[17] E. Basar, *Brain Function and Oscillations* (Springer, Berlin, 1998).
[18] C. Torrence and G. P. Compo, Bull. Am. Meteorol. Soc. **79**, 61 (1998).
[19] D. J. DeShazer, R. Breban, E. Ott, and R. Roy, Phys. Rev. Lett. **87**, 044101 (2001).
[20] M. L. Van Quyen *et al.*, J. Neurosci. Methods **111**, 83 (2001).
[21] K. T. Dolan and A. Neiman, Phys. Rev. E **65**, 026108 (2002).
[22] M. E. J. Newman, Contemp. Phys. **46**, 323 (2005).
[23] F. Takens, in *Dynamical Systems and Turbulence*, 1980, edited by D. A. Rang and L. S. Young, *Lecture Notes in Mathematics*, Vol. 898 (Springer, Berlin, 1981), p. 366.
[24] J. Stark *et al.*, Nonlinear Anal. Theory, Methods Appl. **30**, 5303 (1997).
[25] N. B. Janson, A. G. Balanov, V. S. Anishchenko, and P. V. E. McClintock, Phys. Rev. Lett. **86**, 1749 (2001).
[26] N. B. Janson, A. G. Balanov, V. S. Anishchenko, and P. V. E. McClintock, Phys. Rev. E **65**, 036212 (2002).
[27] A. Brandstater *et al.*, Phys. Rev. Lett. **51**, 1442 (1983).
[28] J. H. Cho, M. S. Ko, Y. J. Park, and C. M. Kim, Phys. Rev. E **65**, 036222 (2002).
[29] H. G. Schuster, *Deterministic Chaos* (VCH, Weinheim, 1998).
[30] R. F. Engle, Econometrica **50**, 987 (1982).
[31] K. Kaneko and I. Tsuda, *Complex Systems: Chaos and Beyond* (Springer, Berlin, 2000).
[32] S. L. Bressler and J. A. S. Kelso, Trends Cogn. Sci. **5**, 26

(2001).
[33] C. van Leeuwen, M. Steyvers, and M. Nooter, J. Math. Psychol. **41**, 319 (1997).
[34] E. Schneidman, M. J. Berry, R. Segev, and W. Bialek, Nature (London) **440**, 1007 (2006).
[35] Y. F. Contoyiannis and F. K. Diakonos, Phys. Lett. A **268**, 286 (2000).
[36] Y. F. Contoyiannis, F. K. Diakonos, and A. Malakis, Phys. Rev. Lett. **89**, 035701 (2002).
[37] H. V. McIntosh, Physica D **45**, 105 (1990).
[38] P. Bak, C. Tang, and K. Wiesenfeld, Phys. Rev. Lett. **59**, 381 (1987).